NUCL SCI TECH (2018) 29:156
https://doi.org/10.1007/s41365-018-0500-3

A study on the excitation functions of ^{60,62}Ni(α,n), ^{60,61}Ni(α,2n), ^{58,64}Ni(α,p), ^{nat}Ni(α,x) reactions

Rıdvan Baldık[1] · Aykut Yılmaz[1]

Received: 8 February 2018 / Revised: 9 May 2018 / Accepted: 9 June 2018 / Published online: 27 September 2018

Abstract The prediction of nuclear cross-section data is crucial, especially in the absence of experimental data or in the difficulty of these experimental data. Nickel (Ni) is an important material in fusion and fission reactor technologies, the production of radionuclides in nuclear medicine, and many other fields. In this study, the excitation functions for ^{60,62}Ni(α,n), ^{60,61}Ni(α,2n), ^{58,64}Ni(α,p), and ^{nat}Ni(α,x) reactions have been investigated by using pre-equilibrium reaction models. The calculations of the excitation functions for the reactions are used with the geometry-dependent hybrid model in ALICE/ASH code and the two-component exciton model in TALYS 1.8 code. The obtained results are compared to each other, and the experimental data are taken from the EXFOR database.

Keywords Nuclear reaction models and methods · Level density · Alpha-induced reactions · ALICE/ASH code · TALYS 1.8 code

1 Introduction

The nuclear cross-section data for particle-induced reaction benefit from the structural materials development in the fusion and fission reactors, medical radioisotope production, and astrophysical applications, etc. Because the obtained nuclear reaction data via experiment have difficulties with regard to both time and financial considerations, the importance of theoretical data has increased. Therefore, theoretical cross-section data are used to determine the optimal energy ranges required for a reaction type and to calculate the radioisotope production yield [1, 2]. The cross-section data can also be used to obtain the radioactive impurities that help to determine isotopically enriched target materials for medical radioisotopes production and in the calculations of astrophysical S factors for nuclear astrophysics reactions, etc. [1, 2]. Therefore, research and development efforts on the nuclear cross-section data have gradually increased in the literature [1, 3–19].

Nuclear reaction models are necessary in order to determine nuclear reaction data and make theoretical calculations. The models are typically required to provide the estimation of the nuclear reaction cross sections. Pre-equilibrium reaction models are frequently used in cross-section calculations for estimating radiation damage and producing radioisotopes, etc. The pre-equilibrium reaction mechanism, which was modeled classically and quantum mechanically, exists between direct and compound reaction types in terms of reaction time [20, 21]. These reactions, which are on timescales of 10^{-20}–10^{-18} s, are induced by light projectiles with incidences above $\sim$ 10 MeV.

Nuclear level density is one of the characteristic properties of all nuclei, and the property is defined as the total number of energy levels per MeV at a certain excitation energy. The level density has an important role in the calculations of the nuclear cross section. There are several models in the literature for the determination of the nuclear level density. A brief summary of these models is given in Sect. 2.3. Therefore, the investigations of different level

✉ Rıdvan Baldık
rbaldik@gmail.com

[1] Department of Physics, Faculty of Arts and Science, Zonguldak Bülent Ecevit University, 67100 Zonguldak, Turkey

densities effects on the nuclear reactions have been performed by some researchers [9, 10, 22–26].

In natural nickel (Ni), five isotopes exist (^{58}Ni % 68,077, ^{60}Ni % 26,223, ^{61}Ni % 1.140, ^{62}Ni % 3.635, and ^{64}Ni % 0.926) [27]. The Ni and its alloys are resistant to high temperatures. Therefore, the Ni and its alloys are used in structural materials for the fusion and fission applications. In addition, the Ni is used in space and nuclear equipment working under radiation, radioisotopes production, astrophysical applications, etc. Nevertheless, the Ni activation data are interesting for the design of accelerator-driven systems and analyzed in thin film activation. The Ni targets are also used in the production of $^{55-58}$Co, ^{62}Zn, and $^{60-62,64}$Cu medical radioisotopes [28–30].

In this study, the excitation functions of ^{60,62}Ni(α,n), ^{60,61}Ni(α,2n), ^{58,64}Ni(α,p), and ^{nat}Ni(α,x) reactions are calculated by using the pre-equilibrium reaction mechanism. The calculations are made by the ALICE/ASH code [31], which was used with the geometry-dependent hybrid (GDH) models, and by the TALYS 1.8 code [20] used with the two-component exciton model. However, in this study, for the first time, the reactions have been handled with the ALICE/ASH and the TALYS 1.8 codes. In addition, the different nuclear level density models effects on the GDH and the two-component exciton models have been investigated for the reactions in the present study. The obtained excitation functions have been discussed and compared with the experimental data [32].

2 Calculations

2.1 ALICE/ASH code

The ALICE/ASH code, which is useful for pre-equilibrium calculations, was developed by Broeders et al. [31]. The ALICE/ASH code includes the calculations of excitation functions, energy and angular distributions of the particles emitted in nuclear reactions, residual nuclear yields, and total inelastic cross sections for particles–nuclei reactions with up to 300 MeV [31]. The pre-equilibrium models are the hybrid and GDH models in the ALICE/ASH code. The hybrid model was formulated by Blann [33] and combines the simplicity of the formulation of the exciton model [34] with the ability to predict the absolute cross sections of the Harp-Miller-Berne model [35]. The GDH model contains the effects of the interactions in the diffuse nuclear surface. The nuclear densities in the GDH model are calculated by averaging over the densities relative to the entrance channel of projectiles, at least for the first projectile and target interaction [36–38].

2.2 TALYS 1.8 code

The TALYS 1.8 code is a computer code that contains the simulation of nuclear reactions for incident particles such as protons, neutrons, photons, deuterons, tritons, ^{3}He, and alpha particles and for target nuclei from Li to Dy in the 1 keV–200 MeV incident particle energy range [20]. The code provides observables of the reaction and a complete description of all the reaction channels [20]. Also, the code can be used for the analysis of basic scientific experiments or generation of nuclear data for applications [20]. In this study, the pre-equilibrium calculations in the TALYS 1.8 code are performed by using the two-component exciton model. The two-component exciton model is another version of the exciton model, where the temporal development of the system can be described by a master equation. The master equation is determined by the exciton numbers separating the neutron and proton excitons [21, 39].

2.3 Nuclear level densities

Two important models for level density approximation were firstly performed by Bethe [40, 41]. The first model was based on the gas system, which consists of non-interacted particles called the Fermi gas model (FGM). The second was the liquid drop model. Hereupon, the conventional shifted Fermi gas was introduced by Erba et al. [42], Newton [43], and Cameron [44]. The excitation energy in the model was changed using the pairing energy parameter (Δ), and the (Δ) and (2Δ) were represented by the shifts for odd mass and even–even nuclei, respectively [45]. The next step for nuclear level density by Gilbert and Cameron was to define the constant temperature (CT) model [46]. The important step includes the corrections of some parameterizations such as dependence on atomic mass effects, shell effects, and odd–even pairing effects. Their formula included a two-component level density formula with energy shifts [45]. To calculate the level density, they used a constant temperature formula for lower energies (for the first energy levels till $\sim$ 10 MeV) and the conventional shifted Fermi gas formula at higher excitation [45–47]. The model is called the constant temperature plus Fermi gas model (CT + FGM), and the only free parameter for this model is the level density parameter. Another simpler and rather effective model is the back-shifted Fermi gas model (BSFGM) [47]. The model, in which all excitation energies are obtained by using the Fermi gas formula, has two free parameters: the level density and the back-shifted energy parameters [45, 47].

The other level density model is the generalized superfluid model (GSM) [48, 49], which is based upon the pairing correlations of the Bardeen-Cooper-Schrieffer

(BCS) theory in the superconductor. Here, the pairing correlations represented a phase transition from superfluid behavior, which strongly influenced the nuclear level density at low energies. However, the model is described by the FGM at high energies [20]. The GSM at high energies is similar to CT + FGM, but at low energies, the GSM is independent of the specific discrete levels and follows the nature of the theory [20].

The level density models used to calculate the cross sections in this study are as follows: The FGM with an energy-independent level density parameter in the ALICE/ASH code is labeled as the FGM 1 in the present study (the model is the default model in the ALICE/ASH code). In this model, the level density parameter (a) is taken as the $a = A/9$. Another option for the FGM in the ALICE/ASH code is the FGM with an energy-dependent level density parameter, and that option in this study is labeled as the FGM 2. The parameter is:

$$a = \tilde{a}\left(1 + \delta W \frac{1 - e^{-\gamma U}}{U}\right). \quad (1)$$

Here, $\tilde{a}$ is the asymptotic level density, γ is the damping parameter, and δW is the shell correction energy. Also, the effective excitation energy (U) in Eq. (1) is determined by $U = E_X - \Delta$, where E_X is the true excitation energy and an empirical parameter, Δ, is the energy shift. However, the level density parameter in Eq. (1) is used for the CT + FGM (default model) and the BSFGM in the TALYS 1.8 code. On the other hand, the level density parameter for the GSM in the ALICE/ASH and TALYS 1.8 codes is as follows:

$$a(U) = \left\{ \begin{array}{ll} \tilde{a}\left(1 + \delta W \dfrac{1 - e^{-\gamma(U' - E_{\mathrm{cond}})}}{U' - E_{\mathrm{cond}}}\right), & U' > U_{\mathrm{cr}} \\ a(U_{\mathrm{cr}}), & U' \leq U_{\mathrm{cr}} \end{array} \right\}, \quad (2)$$

where U' is the effective excitation energy, U_{cr} is the critical energy of the phase transition, and E_{cond} is condensation energy. The extensive reviews for nuclear level density models and the level density parameters can be seen in Refs. [20, 31].

3 Results and discussions

The comparison of the calculated excitation functions for ^{60,62}Ni(α,n), ^{60,61}Ni(α,2n), ^{58,64}Ni(α,p), and ^{nat}Ni(α,x) reactions using the pre-equilibrium reaction models and the available experimental data is presented in Figs. 1, 2, 3, 4, 5, 6, 7, 8, 9, 10, 11, 12 and 13 as a function of the incident alpha energy. The experimental data were taken from the EXFOR data files [32].

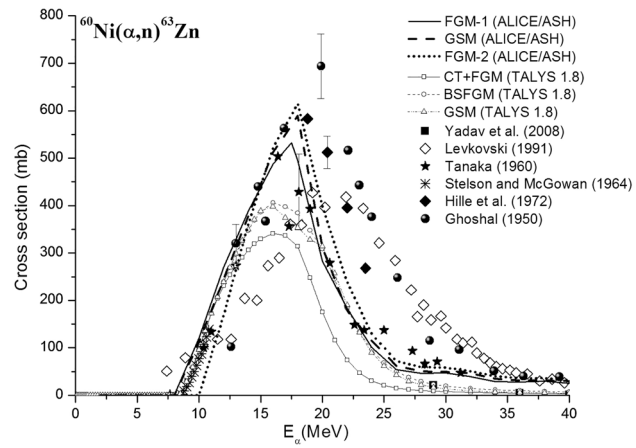

Fig. 1 Comparison of the theoretically calculated excitation functions with experimental data for the ^{60}Ni(α,n)^{63}Zn reaction

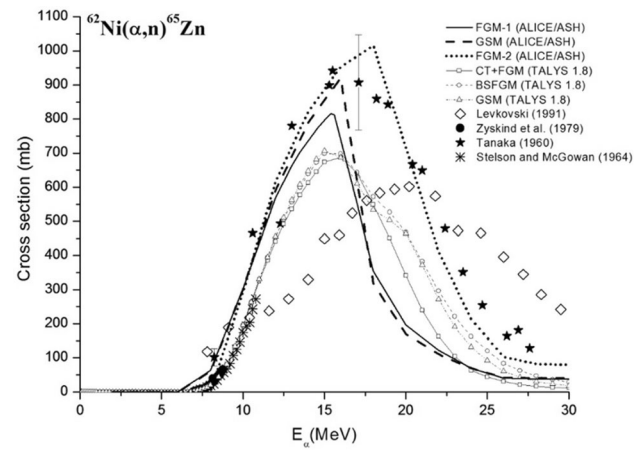

Fig. 2 Comparison of the theoretically calculated excitation functions with experimental data for the ^{62}Ni(α,n)^{65}Zn reaction

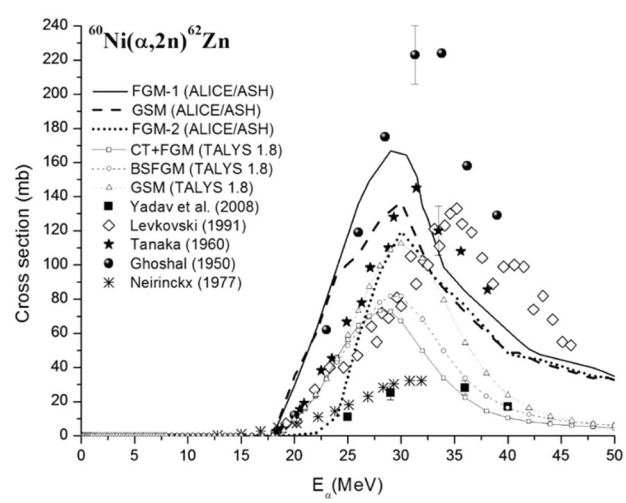

Fig. 3 Comparison of the theoretically calculated excitation functions with experimental data for the ^{60}Ni(α,2n)^{62}Zn reaction

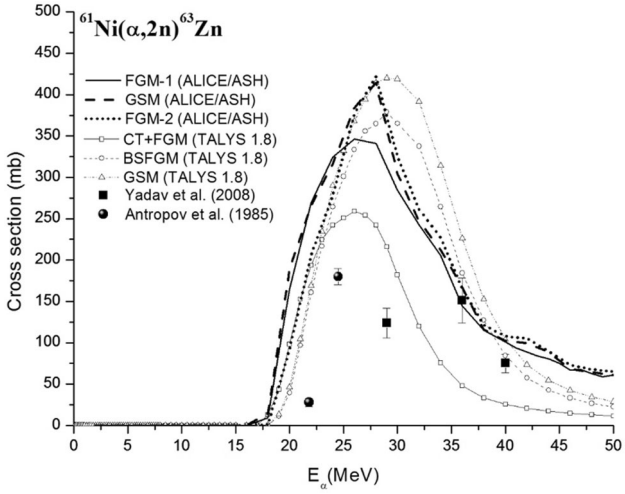

Fig. 4 Comparison of the theoretically calculated excitation functions with experimental data for the ^{61}Ni(α,2n)^{63}Zn reaction

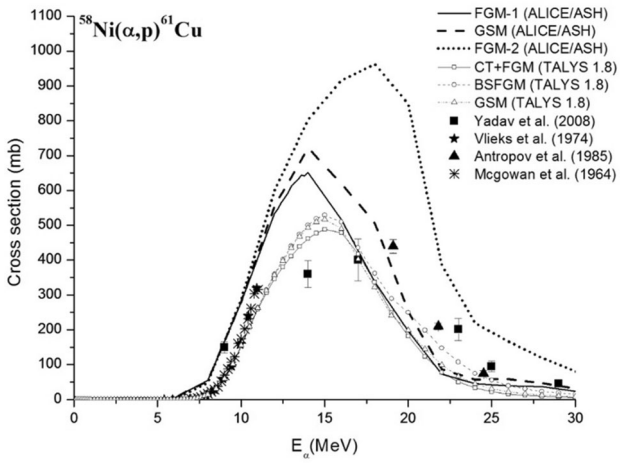

Fig. 5 Comparison of the theoretically calculated excitation functions with experimental data for the ^{58}Ni(α,p)^{61}Cu reaction

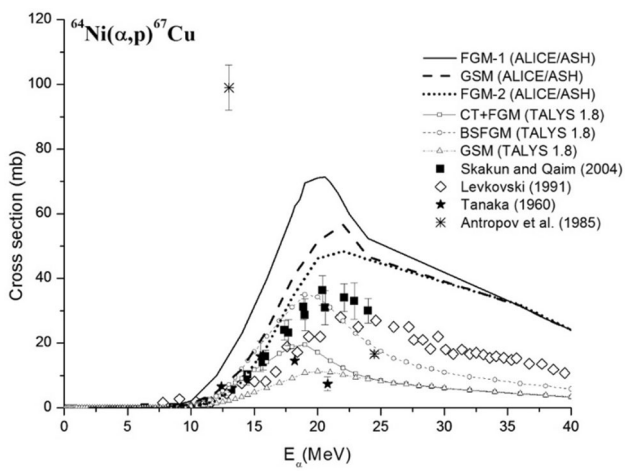

Fig. 6 Comparison of the theoretically calculated excitation functions with experimental data for the ^{64}Ni(α,p)^{67}Cu reaction

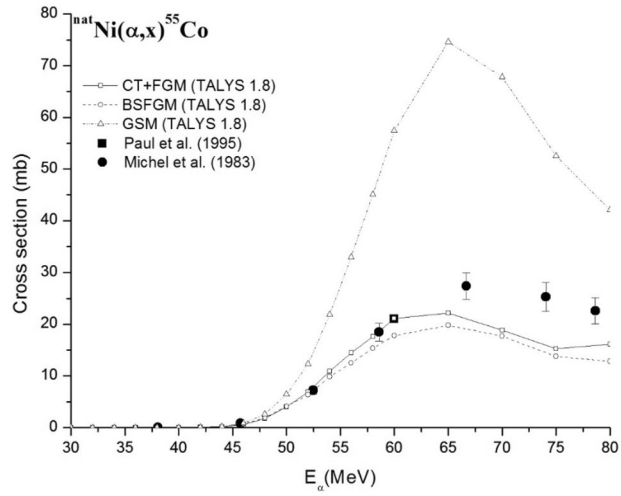

Fig. 7 Comparison of the theoretically calculated excitation functions with experimental data for the ^{nat}Ni(α,x)^{55}Co reaction

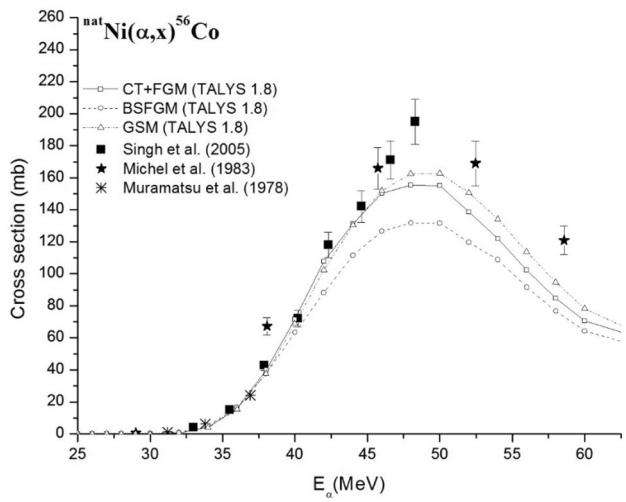

Fig. 8 Comparison of the theoretically calculated excitation functions with experimental data for the ^{nat}Ni(α,x)^{56}Co reaction

3.1 The excitation functions of the ^{60,62}Ni(α,n), ^{60,61}Ni(α,2n), and ^{58,64}Ni(α,p) reactions

All theoretical results for the ^{60}Ni(α,n) reaction are close to each other and the experimental data [50–55] up to ~ 12 MeV incident alpha energy in Fig. 1, except for the FGM 2. The reason for this can be arisen from using the CT formula for low energies in the FGM 2. While the CT approach is used at the excitation energies < 2 MeV in the FGM 2, this approach for the CT + FGM in the two-component exciton model is applied into a low energy range from 0 MeV up to a matching energy, E_M. The matching energy is determined by $E_M = 2.33 + 253/A + \Delta_{CTM}$, where the Δ_{CTM} is the energy shift which is given by $\chi \frac{12}{\sqrt{A}}$ ($\chi = 0$ for odd–odd nuclei, 1 for odd–even

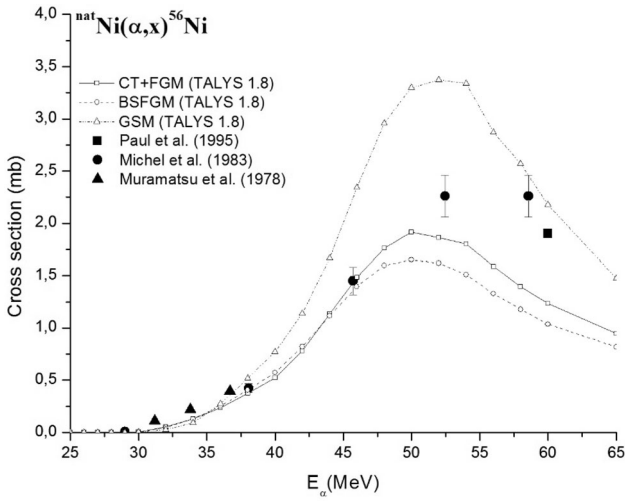

Fig. 9 Comparison of the theoretically calculated excitation functions with experimental data for the ^{nat}Ni(α,x)^{56}Ni reaction

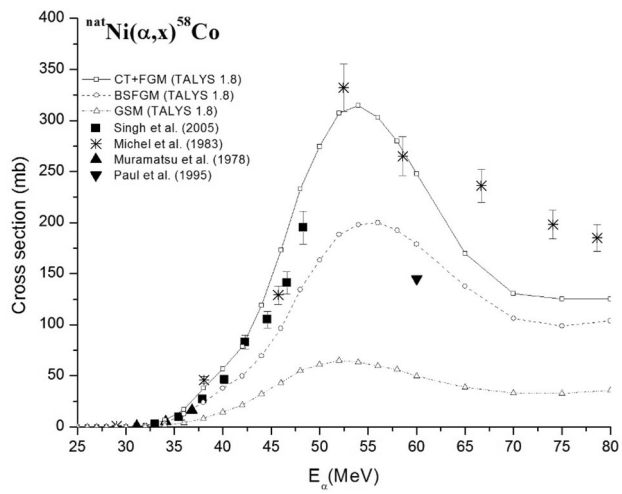

Fig. 10 Comparison of the theoretically calculated excitation functions with experimental data for the ^{nat}Ni(α,x)^{58}Co reaction

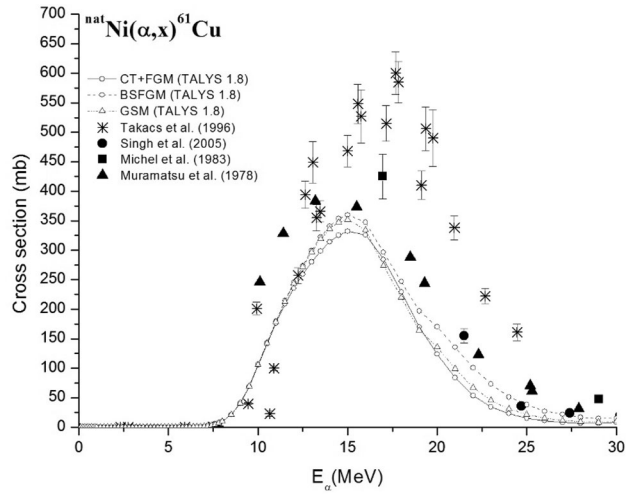

Fig. 11 Comparison of the theoretically calculated excitation functions with experimental data for the ^{nat}Ni(α,x)^{61}Cu reaction

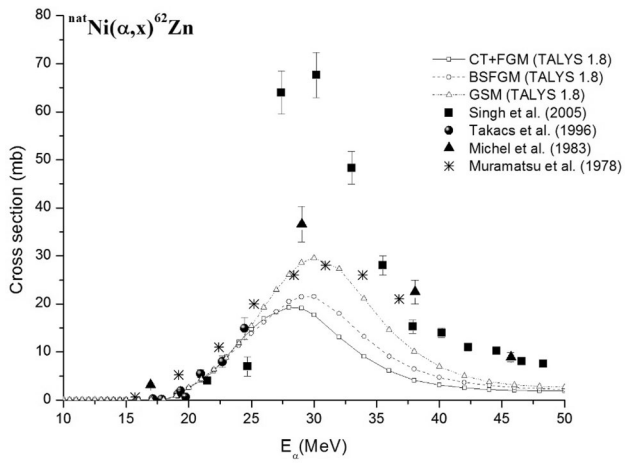

Fig. 12 Comparison of the theoretically calculated excitation functions with experimental data for the ^{nat}Ni(α,x)^{62}Zn reaction

nuclei, 2 for even–even nuclei). The same effect (the CT approach) on the excitation functions of ^{62}Ni(α,n), ^{60,61}Ni(α,2n), and ^{64}Ni(α,p) reactions in Figs. 2, 3, 4 and 6 is seen more or less. In the range of ~ 12–20 MeV incident energy, the obtained excitation functions using the different level density models have different values in Fig. 1. Nevertheless, it can be said that the results for different level density models in the GDH model are generally compatible with the experimental datasets. According to the obtained results above 20 MeV, the closest theoretical results to the experimental datasets are the FGM 2 in the GDH model.

For the ^{62}Ni(α,n) reaction up to 10.8 MeV, the calculated excitation functions using the three level density models in the two-component exciton model are close to each other and in good agreement with the experimental data of Stelson and McGowan [53] and Zyskind et al. [56] in Fig. 2. The excitation functions for the FGM 2 in the GDH model for all incident alpha energies are also in good agreement with the experimental data of Tanaka [52]. Furthermore, the most compatible model with the experimental data in the high incident energy range for this reaction is the FGM 2 in the GDH model. Also, in the literature, the calculations of the excitation function for the ^{62}Ni(α,n) reaction in the incident alpha energy of 6–10 MeV for the CT + FGM model in TALYS 1.6 were conducted by Yıldız and Aydın [1]. The obtained excitation function used for the CT + FGM model in the TALYS 1.8 code for the ^{62}Ni(α,n) reaction in this energy range is similar to that of Yıldız and Aydın.

In Fig. 3, the different level density models for the two-component exciton model are not effective in the excitation functions for the ^{60} Ni(α,2n) reaction up to ~ 25 MeV.

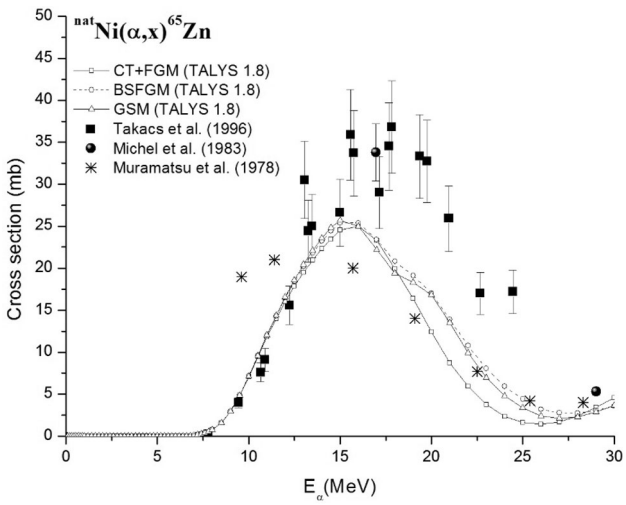

Fig. 13 Comparison of the theoretically calculated excitation functions with experimental data for the $^{nat}Ni(\alpha,x)^{65}Zn$ reaction

The results of the two-component exciton model for this reaction up to ~ 29 MeV are in agreement with the experimental data of Tanaka [52] and Levkovski [51]. In the range of 25–29 MeV, the results of the GSM in the two-component exciton model and the FGM 2 in the GDH model are compatible with the data of Tanaka [52]. After this incident alpha energy, i.e. in the high-energy range, the most compatible model with the experimental data is the FGM 1 in the GDH model. Also, for the $^{61}Ni(\alpha,2n)$ reaction in Fig. 4, the obtained excitation functions used for the GSM and the FGM 2 in the GDH model are close to each other and have higher values than those of the FGM 1. On the other hand, the results of the BSFGM and the GSM in the two-component exciton model are higher than those of the CT + FGM. For this reaction, the results of the FGM 1 in the GDH model at the 36 MeV and the BSFGM in the two-component exciton model at the 40 MeV are in good agreement with the Yadav et al. data [50].

The calculated excitation functions used in the different level density models in the two-component exciton model are close to each other and are in good agreement with the experimental data [53, 57, 58] up to ~ 12 MeV, except for one set of data by Yadav et al. [50] at 9 MeV (in Fig. 5). Also, the excitation functions of the $^{58}Ni(\alpha,p)$ reaction to the production of ^{61}Cu were analyzed by Aslam and Qaim using the EMPIRE and the BSFGM in the TALYS 1.4 codes [59]. When the Aslam and Qaim study and the present one for the ^{58}Ni (α,p) reaction are compared, the results are close to each other. For the $^{64}Ni(\alpha,p)$ reaction, the calculated excitation functions using the GSM in the two-component exciton model are more compatible with experimental data [51, 52, 58, 60] than those of other models in Fig. 6. Also, Levkovski's experimental data for this reaction and $^{60,62}Ni(\alpha,n)$, $^{60}Ni(\alpha,2n)$, and $^{64}Ni(\alpha,p)$ reactions in Figs. 1, 2, 3 and 6 are considerably different in behavior than those of other experimental data. The reason of this may be due to Levkovski's use of a different target holder, which was a rotating target for the simultaneous irradiation of a few foils [51].

The optimum energy range for a nuclear reaction is the incident particle energy range corresponding to the highest cross sections. In this study, the optimum energy ranges for the $^{60,62}Ni(\alpha,n)$, $^{60}Ni(\alpha,2n)$, $^{61}Ni(\alpha,2n)$, $^{58}Ni(\alpha,p)$, and $^{64}Ni(\alpha,p)$ reactions were obtained as $E_\alpha = 14 \rightarrow 19$ MeV, $E_\alpha = 15 \rightarrow 18$ MeV, $E_\alpha = 26 \rightarrow 32$ MeV, $E_\alpha = 14 \rightarrow 17$ MeV, and $E_\alpha = 18 \rightarrow 21$ MeV, respectively. Also, the product nuclei of the $^{60,62}Ni(\alpha,n)$ $^{60,61}Ni(\alpha,2n)$, and $^{58,64}Ni(\alpha,p)$ reactions are radioactive: ^{62}Zn ($T_{1/2}$ = 9.19 h and β^+ decay), ^{63}Zn ($T_{1/2}$ = 38.47 min and β^+ decay), ^{65}Zn ($T_{1/2}$ = 243.93 days and β^+ decay), ^{61}Cu ($T_{1/2}$ = 3.33 h and β^+ decay), and ^{67}Cu ($T_{1/2}$ = 61.83 h and β^- decay) [27].

3.2 The excitation functions of the $^{nat}Ni(\alpha,x)$ reactions

The obtained excitation functions using the TALYS 1.8 code for the $^{nat}Ni(\alpha,x)$ reactions are presented in Figs. 7, 8, 9, 10, 11, 12 and 13. The optimum energy ranges for the $^{nat}Ni(\alpha,x)$ reactions in this study are obtained as $E_\alpha = 14 \rightarrow 65$ MeV. The different nuclear level density models' effect on the $^{nat}Ni(\alpha,x)$ reactions prominently arises after ~ 20–30 MeV incident alpha energies. In addition, it is difficult to state that a single model could substitute for the experimental data. Therefore, the calculated excitation functions using the CT + FGM for the $^{nat}Ni(\alpha,x)^{55}Co$, the $^{nat}Ni(\alpha,x)^{58}Co$, $^{nat}Ni(\alpha,x)^{61}Cu$, and the GSM for the $^{nat}Ni(\alpha,x)^{56}Co$ and the $^{nat}Ni(\alpha,x)^{62}Zn$, and the BSFGM and GSM together for the $^{nat}Ni(\alpha,x)^{65}Zn$ are compatible with the experimental data [61–65]. For the $^{nat}Ni(\alpha,x)^{56}Ni$ reaction, while the CT + FGM results are in good agreement with experimental data [61, 62, 64] in the low energy range, the GSM results are compatible with the experimental data in the high energy range. The cross section for the $^{nat}Ni(\alpha,x)^{61}Cu$ reaction in the optimum energy range has the highest value among $^{nat}Ni(\alpha,x)$ reactions. Also, the product nuclei of these reactions are radioactive (β^+ decay): ^{55}Co ($T_{1/2}$ = 17.53 h), ^{56}Co ($T_{1/2}$ = 77.24 days), ^{56}Ni ($T_{1/2}$ = 6.08 days), ^{58}Co ($T_{1/2}$ = 70.86 days), ^{61}Cu ($T_{1/2}$ = 3.33 h), ^{62}Zn ($T_{1/2}$ = 9.19 h), and ^{65}Zn ($T_{1/2}$ = 243.93 days) [27].

4 Conclusion

The excitation functions of $^{60,62}Ni(\alpha,n)$, $^{60,61}Ni(\alpha,2n)$, $^{58,64}Ni(\alpha,p)$, and $^{nat}Ni(\alpha,x)$ reactions are obtained by using the different nuclear level density models effects on the

GDH and the two-component exciton models. According to the results, while nuclear level density models have an effect on the excitation functions of the handled reaction in the low incident energy range, it is relatively small, and this influence is more visible in the high incident energy range. Therefore, in this study, it is hard to state that a single model can explain the pre-equilibrium cross sections of the alpha incident reactions. Furthermore, the results of the two models are different although the GDH and the two-component exciton models are based on the exciton model. The reason for this originates in the difference between the GDH model and the exciton model. Namely, while the GDH model is an independent particle model and also an inclusive model, the exciton model is a system approximation and exclusive model [66]. However, mixing a complete particle–hole configuration within exciton states is assumed in the exciton model, whereas the GDH model assumes no configuration mixing at all [66, 67]. In addition, the initial exciton number and the internal decay rates in two models are crucial and adjustable parameters, so it is difficult to make an experimental verification as to which of the models is correct [68]. The results evaluated in the present paper may be used for better understanding of the (α,x) reactions.

References

1. E. Yildiz, A. Aydin, Calculation of cross-sections and astrophysical S-factors for ^{62}Ni(α,n) and ^{62}Ni(α,γ) reactions of structural fusion material nickel. J. Fusion Energy **35**, 605–607 (2016). https://doi.org/10.1007/s10894-016-0079-9
2. F. Szelecsényi, Measurement of cross sections of proton induced nuclear reactions on Ti, Ni, Zn, Cd and Au up to 30 MeV and their applications in radioisotope (2009)
3. E. Tel, A. Kara, Neutron, proton and alpha emission spectra of nickel isotopes for proton induced reactions. J. Fusion Energy **31**, 257–261 (2012). https://doi.org/10.1007/s10894-011-9470-8
4. E. Tel, Study on some structural fusion materials for (n, p) reactions up to 30 MeV energy. J. Fusion Energy **29**, 332–336 (2010). https://doi.org/10.1007/s10894-010-9285-z
5. E. Tel, C. Durgu, N.N. Akti, Ş. Okuducu, Calculations of excitation functions of some structural fusion materials for (n, t) Reactions up to 50 MeV energy. J. Fusion Energy **29**, 290–294 (2010). https://doi.org/10.1007/s10894-010-9277-z
6. E. Tel, S. Akca, M. Sahan et al., The comparison of (n, p), (n, α), (n,2n) and (α, n) reaction cross-sections for ^{7}Li and ^{9}Be target nuclei. J. Fusion Energy. **35**(4), 709–714 (2016). https://doi.org/10.1007/s10894-016-0094-x
7. B. Demir, H. Sarpün, A. Kaplan et al., Double differential cross section and stopping power calculations of light charged particle emission for the structural fusion materials ^{50,52}Cr. J. Fusion Energy **34**, 808–816 (2015). https://doi.org/10.1007/s10894-015-9889-4
8. H. Sarpün, A. Aydın, A. Kaplan et al., Double differential charged particle emission cross sections and stopping power calculations for structural fusion materials ^{58,60}Ni. J. Fusion Energy **34**, 1306–1313 (2015). https://doi.org/10.1007/s10894-015-9961-0
9. A. Aydin, H. Pekdogan, A. Kaplan et al., Comparison of level density models for the ^{60,61,62,64}Ni(p, n) reactions of structural fusion material nickel from threshold to 30 MeV. J. Fusion Energy **34**, 1105–1108 (2015). https://doi.org/10.1007/s10894-015-9927-2
10. B. Demir, A. Kaplan, V. Çapalı et al., Neutron production cross-section and Geant4 calculations of the structural fusion material ^{59}Co for (α, xn) and (γ, xn) reactions. J. Fusion Energy **34**, 636–641 (2015). https://doi.org/10.1007/s10894-015-9860-4
11. A. Kaplan, V. ÇapalI, H. Özdoğan et al., (^{3}He, xn) reaction cross-section calculations for the structural fusion material ^{181}Ta in the energy range of 14–75 MeV. J. Fusion Energy **33**, 510–515 (2014). https://doi.org/10.1007/s10894-014-9705-6
12. F.A. Uğur, E. Tel, A.A. Gökçe, A study on ^{19}F(n, α) reaction cross section. J. Fusion Energy **32**, 414–418 (2013). https://doi.org/10.1007/s10894-012-9587-4
13. E. Tel, F.A. Ugur, A.A. Gokce, Alpha induced reaction cross section calculations of tantalum nucleus. J. Fusion Energy **32**, 304–310 (2013). https://doi.org/10.1007/s10894-012-9550-4
14. H. Aytekin, O. Artun, R. Baldık, Cross-section calculations of proton induced (p, n) and (p,2n) reactions for production of diagnostic ^{67}Ga, ^{81}Rb, ^{111}In, ^{123,124}I, ^{123}Cs and ^{123}Xe radioisotopes. J. Radioanal. Nucl. Chem. **298**, 95–103 (2013). https://doi.org/10.1007/s10967-013-2478-y
15. R. Baldık, H. Aytekin, E. Tel, Equilibrium and pre-equilibrium calculations of cross-sections of (p, xn) reactions on ^{89}Y, ^{90}Zr and ^{94}Mo targets used for the production of ^{89}Zr, ^{90}Nb and ^{94}Tc positron-emitting radionuclides. Pramana **80**, 251–261 (2013). https://doi.org/10.1007/s12043-012-0472-5
16. R. Baldık, H. Aytekin, O. Artun, Investigation of excitation functions for (n, 2n) reactions on some samarium, europium and gadolinium isotopes in the mass region $144 \leq A \leq 160$. Mod. Phys. Lett. A **29**, 1450074 (2014). https://doi.org/10.1142/S0217732314500746
17. H. Aytekin, R. Baldik, Pre-equilibrium and equilibrium calculations of (n, p) reactions on ^{32}S, ^{64}Zn, ^{67}Zn, ^{89}Y, ^{90}Zr and ^{153}Eu targets used for production of ^{32}P, ^{64}Cu, ^{67}Cu, ^{89}Sr, ^{90}Y and ^{153}Sm therapeutic radionuclides. Ann. Nucl. Energy **53**, 439–446 (2013). https://doi.org/10.1016/j.anucene.2012.09.028
18. R. Baldik, A. Dombayci, Investigation of the production of ^{68}Ga using pre-equilibrium models. Appl. Radiat. Isot. **113**, 10–17 (2016). https://doi.org/10.1016/j.apradiso.2016.04.002
19. O. Artun, H. Aytekin, Calculation of excitation functions of proton, alpha and deuteron induced reactions for production of medical radioisotopes $^{122-125}$I. Nucl. Instrum. Meth. B. **345**, 1–8 (2015). https://doi.org/10.1016/j.nimb.2014.12.029
20. A. Koning, S. Hilaire, S. Goriely, Talys-1.8 A Nuclear Reaction Program, (2015). http://www.talys.eu/fileadmin/talys/user/docs/talys1.8.pdf. Accessed 2017.
21. A.J. Koning, M.C. Duijvestijn, A global pre-equilibrium analysis from 7 to 200 MeV based on the optical model potential. Nucl. Phys. A **744**, 15–76 (2004). https://doi.org/10.1016/j.nuclphysa.2004.08.013
22. M. Yiğit, E. Tel, H. Sarpün, Excitation function calculations for α + ^{93}Nb nuclear reactions. Nucl. Instrum. Methods Phys. Res. Sect. B Beam Interact. Mater. Atoms **385**, 59–64 (2016). https://doi.org/10.1016/j.nimb.2016.08.019
23. A. Kara, T. Korkut, M. Yigit et al., Modelling study on production cross sections of ^{111}In radioisotopes used in nuclear medicine. Kerntechnik **80**, 270–274 (2015). https://doi.org/10.3139/124.110527
24. M. Eslami, T. Kakavand, M. Mirzaii, Theoretical approach to study the light particles induced production routes of ^{22}Na. Ann.

Nucl. Energy **83**, 14–24 (2015). https://doi.org/10.1016/j.anucene.2015.04.004
25. I.H. Sarpün, A. Aydin, A. Kaplan et al., Comparison of fission barrier and level density models for (α, f) reaction of some heavy nuclei. Ann. Nucl. Energy **70**, 175–179 (2014). https://doi.org/10.1016/j.anucene.2014.03.017
26. M. Yiğit, A. Kara, Model-based predictions for nuclear excitation functions of neutron-induced reactions on $^{64,66-68}$Zn targets. Nucl. Eng. Technol. **49**, 996–1005 (2017). https://doi.org/10.1016/j.net.2017.03.006
27. G. Audi, F.G. Kondev, M. Wang et al., NUBASE2012 evaluation of nuclear properties. Nucl. Data Sheets **36**, 1157–1286 (2012). https://doi.org/10.1016/j.nds.2014.06.127
28. S.J. Zinkle, N.M. Ghoniem, Operating temperature windows for fusion reactor structural materials. Fusion Eng. Des. **51–52**, 55–71 (2000). https://doi.org/10.1016/S0920-3796(00)00320-3
29. N. Amjed, F. Tarkanyi, A. Hermanne et al., Activation cross sections of proton induced reactions on natural Ni up to 65MeV. Appl. Radiat. Isot. **92**, 73–84 (2014). https://doi.org/10.1016/j.apradiso.2014.06.008
30. R.D. Neirinckx, Excitation function for the ^{60}Ni(a,2n)^{62}Zn reaction and production of ^{62}Zn bleomycin. Int. J. Appl. Radiat. Isot. **28**, 808–809 (1977). https://doi.org/10.1016/0020-708X(77)90121-1
31. M. Broeders, C.H.M. Yu Konobeyev, A. Yu Korovin et al., *ALICE/ASH pre-compound and evaporation model code system for calculation of excitation functions, energy and angular distributions of emitted particles in nuclear reactions at intermediate energies* (Forschungszentrum Karlsruhe, Karlsruhe, 2006), pp. 1–230. https://publikationen.bibliothek.kit.edu/270064701
32. EXFOR, EXFOR/CSISRS (Experimental Nuclear Reaction Data File), EXFOR/CSISRS (Experimental Nucl. React. Data File). (2017)
33. M. Blann, Hybrid model for pre-equilibrium decay in nuclear reactions. Phys. Rev. Lett. **27**, 337–340 (1971)
34. J.J. Griffin, Statistical model of intermediate structure. Phys. Rev. Lett. **17**, 478 (1966). https://doi.org/10.1103/PhysRevLett.17.478
35. B.J. Harp, G.D. Miller, J.M. Berne, Attainment of statistical equilibrium in excited nuclei. Phys. Rev. **165**, 1166–1169 (1968). https://doi.org/10.1103/PhysRev.165.1166
36. M. Blann, A. Mignerey, Pre-equilibrium decay at moderate excitations and the hybrid model. Nucl. Phys. A **186**, 245–256 (1972). https://doi.org/10.1016/0375-9474(72)90043-7
37. M. Blann, Preequilibrium decay. Annu. Rev. Nucl. Sci. **25**, 123–166 (1975). https://doi.org/10.1146/annurev.ns.25.120175.001011
38. M. Blann, H.K. Vonach, Global test of modified precompound decay models. Phys. Rev. C **28**, 1475–1492 (1983). https://doi.org/10.1103/PhysRevC.28.1475
39. C. Kalbach, Two-component exciton model: basic formalism away from shell closures. Phys. Rev. C **33**, 818–833 (1986). https://doi.org/10.1103/PhysRevC.33.818
40. H.A. Bethe, An attempt to calculate the number of energy levels of a heavy nucleus. Phys. Rev. **50**, 332–341 (1936). https://doi.org/10.1103/PhysRev.50.332
41. H.A. Bethe, Nuclear physics B. nuclear dynamics, theoretical. Rev. Mod. Phys. **9**, 69–244 (1937). https://doi.org/10.1103/RevModPhys.9.69
42. E. Erba, U. Facchini, E. Saetta, Menichella, Statistical emission in nuclear reactions and nuclear level density (*). Il Nuovo Cimento **22**, 1237–1260 (1961). https://doi.org/10.1007/BF02786895
43. T.D. Newton, Shell effects on the spacing of nuclear levels. Can. J. Phys. **34**, 804–829 (1956). https://doi.org/10.1139/p56-090
44. A. Cameron, Nuclear level spacings. Can. J. Phys. **36**, 1040–1057 (1958). https://doi.org/10.1139/p58-112
45. M. Guttormsen, M. Hjorth-Jensen, E. Melby et al., Energy shifted level densities in rare earth region. Phys. Rev. C **61**, 067302 (2000). https://doi.org/10.1103/PhysRevC.61.067302
46. A. Gilbert, A.G.W. Cameron, A composite nuclear-level density formula with shell corrections. Canadian J. Phys. **43**(8), 1446–1496 (1965). https://doi.org/10.1139/p65-139
47. W. Dilg, W. Schantl, H. Vonach, M. Uhl, Level density parameters for the back-shifted fermi gas model in the mass range $40 < A < 250$. Nucl. Phys. A. **217**, 269–298 (1973). https://doi.org/10.1016/0375-9474(73)90196-6
48. A.V. Ignatyuk, K.K. Istekov, G.N. Smirenkin, The role of collective effects for nuclear level density systematics. Yad. Fiz. **29**, 875 (1979)
49. A.V. Ignatyuk, J.L. Weil, S. Raman et al., Density of discrete levels in ^{116}Sn. Phys. Rev. C **47**, 1504–1513 (1993). https://doi.org/10.1103/PhysRevC.47.1504
50. A. Yadav, P.P. Singh, M.K. Sharma et al., Large pre-equilibrium contribution in α+^{nat}Ni interactions at ∼ 8–40 MeV. Phys. Rev. C **78**, 044606 (2008). https://doi.org/10.1103/PhysRevC.78.044606
51. V.N. Levkovski, Cross sections of medium mass nuclide activation (*A*=40-100) by medium energy protons and alpha-particles (*E*=10-50 MeV), Act.Cs.By Protons and Alphas, Moscow, 1991
52. S. Tanaka, Reactions of nickel with alpha-particles. J. Phys. Soc. Jpn. **15**, 2159–2167 (1960). https://doi.org/10.1143/JPSJ.15.2159
53. P.H. Stelson, F.K. McGowan, Cross sections for (alpha, n) reactions for medium- weight nuclei. Phys. Rev. **133**, B911–B919 (1964). https://doi.org/10.1103/PhysRev.133.B911
54. W. Hille, M. Hille, P. Uhl et al., Excitation functions of (p, n) and (a, n) reactions on Ni, Cu and Zn. Nucl. Phys. A **198**, 625–640 (1972). https://doi.org/10.1016/0375-9474(72)90713-0
55. S.N. Ghoshal, An experimental verification of the theory of compound nucleus. Phys. Rev. **80**, 939–942 (1950). https://doi.org/10.1103/PhysRev.80.939
56. J.L. Zyskind, J.M. Davidson, M.T. Esat et al., Competition cusps in (alpha, gamma) reactions. Nucl. Phys. A **331**, 180–192 (1979). https://doi.org/10.1016/0375-9474(79)90308-7
57. A.E. Vlieks, J.F. Morgan, S.L. Blatt, Total cross sections for some (α, n) and (α, p) reactions in medium-weight nuclei. Nucl. Phys. A **224**, 492–502 (1974). https://doi.org/10.1016/0375-9474(74)90551-X
58. G.I.Y. Antropov A.E., Zarubın P.P., Aleksandrov YU.A., Cross sections measurements of (p,n),(a,pn),(a,xn) reactions on nuclei Middle Atomic Weight, in *35th Conference on Nuclear Spectroscopy and Nuclear Structure, Leningrad*, 1985, p. 369
59. M.N. Aslam, S.M. Qaim, Nuclear model analysis of excitation functions of proton, deuteron and α-particle induced reactions on nickel isotopes for production of the medically interesting copper-61. Appl. Radiat. Isot. **89**, 65–73 (2014). https://doi.org/10.1016/j.apradiso.2014.02.007
60. Y. Skakun, S.M. Qaim, Excitation function of the ^{64}Ni(α, p)^{67}Cu reaction for production of ^{67}Cu. Appl. Radiat. Isot. **60**, 33–39 (2004). https://doi.org/10.1016/j.apradiso.2003.09.003
61. R.L. Paul, L.J. Harris, P.A.J. Englert et al., Production of cosmogenic nuclides in thick targets by alpha bombardment Part I—short-lived radioisotopes. Nucl. Inst. Methods Phys. Res. B. **100**, 464–470 (1995). https://doi.org/10.1016/0168-583x(95)00355-x
62. R. Michel, G. Brinkmann, R. Stock, Integral excitation functions of alpha-induced reactions on titanium, iron and nickel. Radiochim. Acta **32**, 173–189 (1983). https://doi.org/10.1524/ract.1983.32.4.173
63. N.L. Singh, S. Mukherjee, M.S. Gadkari, Excitation functions of alpha induced reactions on natural nickel up to 50 MeV. Int. J. Mod. Phys. E **14**, 611–629 (2005). https://doi.org/10.1142/S021830130500348X

64. H. Muramatsu, E. Shirai, H. Nakahara et al., Alpha particle bombardments of natural nickel target for the production of ^{61}Cu. Appl. Radiat. Isot. **29**, 611–614 (1978). https://doi.org/10.1016/0020-708X(78)90094-7
65. S. Takacs, F. Tarkanyi, Z. Kovacs, Excitation function of alpha-particle induced nuclear reactions on natural nickel. Nucl. Instrum. Methods B **113**, 424–428 (1996). https://doi.org/10.1016/0168-583X(95)01349-0
66. H. Gruppelaar, P. Nagel, P.E. Hodgson, Pre-equilibrium processes in nuclear reaction theory: the state of the art and beyond. La Riv. Del Nuovo Cim. Ser. **3**(9), 1–46 (1986). https://doi.org/10.1007/BF02725961
67. J. Bisplinghoff, Configuration mixing in preequilibrium reactions: a new look at the hybrid-exciton controversy. Phys. Rev. C **33**, 1569–1580 (1986). https://doi.org/10.1103/PhysRevC.33.1569
68. J. Ernst, J.R. Rao, A unified model of preequilibrium decay. Zeitschrift für Physik A Hadrons and Nuclei **281**, 129–135 (1977). https://doi.org/10.1007/BF01408624